Nanotechnology **17** (2006) 1871–1877 doi:10.1088/0957-4484/17/8/011

Drastic increase in the second-order optical susceptibilities for monodisperse In_2O_3 nanocrystals incorporated into PMMA matrices

I V Kityk[1], J Ebothé[2], Qingsheng Liu[3], Zhaoyong Sun[3] and Jiye Fang[3]

[1] J Dlugosz University Czestochowa, Aleja Armii Krajowej 13/15, Czestochowa, Poland
[2] Laboratoire de Microscopies and d'Etude de Nanostructures, Equipe d'Accueil N3799, BP 138, Universite de Reims, 21 rue Clément Ader, 51685 Reims Cedex 02, France
[3] Department of Chemistry and AMRI, University of New Orleans, New Orleans, LA 70148, USA

Received 2 November 2005
Published 15 March 2006
Online at stacks.iop.org/Nano/17/1871

Abstract
Using photoinduced second-order non-linear optical methods, we have determined that monodisperse In_2O_3 nanocrystals of size ∼11–24 nm incorporated into poly(methyl methacrylate) (PMMA) matrices possess significant second-order optical susceptibilities up to 17 pm V^{-1} at $\lambda = 1.76\ \mu$m; this is almost one order higher than that of traditional nanolayers of In_2O_3. A substantial increase in the corresponding susceptibilities is dependent on a relatively high monodispersion of the nanocrystals. Calculations such as quantum chemical, molecular dynamics and band structure simulations of interfaces indicate that the principal role in the observed non-linear optical effects is played by interfaces on the borders separating the nanocrystals and the surrounding host polymer matrix. In order to clarify a role of the monodispersion and that of the surfaces, additional experiments were carried out using samples with a larger size-distribution of nanocrystals and highly polarized photopolymers of oligoethercrylates as the host matrix. A drastic decrease in the effective optical nonlinearity in these two cases further supports the crucial role of the nanointerfaces.

(Some figures in this article are in colour only in the electronic version)

1. Introduction

An enhanced property can be observed in nanophase materials, such as semiconducting nanocrystals (NCs) for application in non-linear optics (NLO) and quantum electronics, due to the quantum-confined size-dependent electronic and optical properties of these materials [1, 2]. These materials have received much attention during the last decade. This interest is technological, for immediate application in areas of electronics and communications [3–6], and purely fundamental, due to the specific properties of these materials [7, 8]. Quantum confinement dominates the material properties, depending on their particle size and shape topology. The nanoscale-confined effects of the particles are traditionally considered to be detectable when the particle sizes are below 8–10 nm [9]. In such cases, **k**-space bulk-like dispersion disappears and discrete excitonic-like nanolevels occur within the forbidden energy gap [10].

However, there exists a large class of intermediate semiconducting crystallites with average sizes of ∼10–50 nm which may be classified as large sized nanocrystallites (LSNC). For such cases we have a coexistence of typical bulk-like properties (possessing energy **k**-dispersion due to translation symmetry) disturbed by thin near-surface boundary interfaces with a thickness of about 1.5–2.5 nm. Such properties can be useful for different applications, particularly for sensor

applications [11], light emitting devices [12], solar cells, light modulators and deflectors [13].

The quantum-confined boundary interfaces possessing bulk-like as well as dot-like quantized excitonic properties can also be of importance for different optical phenomena, particularly for NLO phenomena due to the large charge density gradients and large values of the NLO susceptibilities [14]. Reconstructed interface boundary sheets with a thickness of 1.5–2.5 nm, separating the bulk-like crystallites and surrounding amorphous-like or disordered background, may cause these features. Very often this fact is neglected, missing an opportunity for investigating further applications.

The principal parameter for a LSNC is the ratio between the thickness of the reconstructed boundary layer (sheet) and the total effective diameter of the particular nanocrystal (NC). Coexistence of bulk-like long-range ordering possessing **k**-space dispersion, large effective mass, low carrier mobility and quantum size-confined layers having substantial spectral blue shift, opens a rare possibility to exploit the electron parameters within the same crystallites.

As a separate topic it is necessary to consider the role of different LSNC matrices (polymers, glasses and amorphous-like materials) in the optoelectronic properties of NCs. The surrounding background plays a crucial role in the application of the particular LSNC chromophores as materials for optoelectronic devices. The influence of the surrounding matrix on the band energy dispersion, effective masses, carrier mobility, values of dipole moments and corresponding optical susceptibilities requires more detailed consideration. In addition the role of the phonon and quasi-phonon subsystems may be crucial, including a possible quantization of these boson sub-systems [15].

We have chosen In_2O_3 semiconductor NCs. These materials are well known as perfect materials for transparent electrodes and possess good optical properties in the visible spectral range. Recently it was discovered that sufficiently good NLO effects originated from the borders separating these films and the substrate [16]. Following these results and the general concept of LSNCs, in the present work we explore the possibility of using the large-sized In_2O_3 NCs as non-linear optical materials. One of advantages of the selected materials compared with other semiconducting materials like ZnO, ZnS, GaN etc is the fact that their size distribution can made fairly monodisperse and tunable compared with nanocrystallites of traditional ferroelectrics such as $LiNbO_3$, $BaTiO_3$, $KTiOPO_4$ or $Bi_{12}SiO_{20}$, sillenites, borates, KH_2PO_4 and other complex oxide systems. Although their optical nonlinearity in the bulk states is higher, which is the general case for many oxide materials [17], it might be technologically difficult to use this property in nanocrystallites due to the presence of octahedral structural fragments which restrict the technological opportunities for low size dispersion.

The second-order optical effects in cubic In_2O_3 bulk crystals are not usually observed in perfect samples. In order to observe the corresponding second-order NLO response, particularly in optical second harmonic generation (SHG), it is necessary to create sufficiently large electrostatic potential space gradients. As an example, in [18] a large SHG signal originated from the nanointerfaces separating In_2O_3 crystalline films and the substrate. It was shown that the NLO effect originated due to the high space gradients effectively varying the band dispersion within several nanometres. In the case of semiconductors, this may make a major contribution to the NLO effects described by the third-order polar tensors requiring non-centrosymmetric charge density. This is different in principle from the effect observed for metallic nanoparticles [19], where the main contribution is due to 'dielectric enhancement' and surface plasmon resonance. Another important factor that is determined by the surrounding polymer matrix is the change of dipolar interactions on the borders separating semiconducting nanoparticles and host polymers [20].

Section 2 of this paper described the details of sample preparation and the NLO (photoinduced SHG) measurement set-up. Section 3 presents the principal results of the NLO measurements. The results are interpreted within a framework of band energy structure calculations on the NC borders and corresponding space charge density distribution.

2. Experimental and characterization method

2.1. Synthesis of In_2O_3 nanocrystals

In_2O_3 LSNCs were synthesized in a hot hexadecane solution under an argon stream using a method reported previously [21]. Typically, the proper amounts of indium acetate, oleylamine and oleic acid were introduced into hexadecane in a three-necked flask equipped with a condenser. All of the starting materials were employed as-received from Aldrich without further purification. The reaction system was vacuumed at room temperature for 15 min and subsequently at 110 °C for 15 min. Trimethylamine N-oxide (TMNO) was then added into this vigorously stirred mixture at 110 °C under an argon stream. The reaction temperature was further increased to 120 °C. After a reaction for 1 h under agitation and argon protection, the temperature was further increased to 290 °C at a rate of 10 °C min^{-1} for an additional 35 min reflux. The products were cooled to room temperature by rapidly removing the heat source, and isolated by adding a sufficient amount of ethanol and separating with centrifugation. After a post-treatment involving size-selective precipitation, the monodisperse In_2O_3 NCs were stored in hexane or toluene.

2.2. Sample preparation

In order to investigate various characteristics, these In_2O_3 colloids were self-assembled on TEM grids and on a surface of a single-crystalline Si wafer for morphological characterization, using a transmission electron microscope (JEOL 2010), and for phase identification, using an x-ray diffractometer (Philips X-pert system). Light scattering experiments were conducted on a DynaPro 99 molecular sizing instrument. The hexane solvent was dried and In_2O_3 NCs were redispersed into poly(methyl methacrylate) (PMMA) chloroform solution at a concentration of ∼4.3% (by weight) for non-linear optical measurements. Independently, the samples were incorporated into photopolymer oligoetheracrylate matrices. These possess substantially higher dipole moments which substantially modify the surface properties of the incorporated chromophore [22], and preparation of the samples was done using UV-induced solidification. The samples for the photopolymer matrices were prepared in the same weighting ratios as in the case of the PMMA matrices.

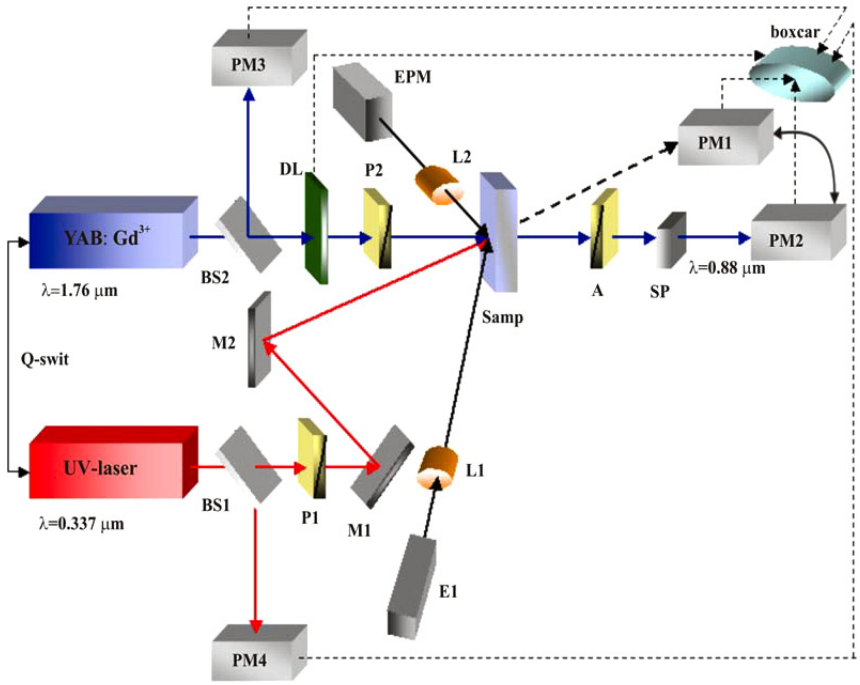

Figure 1. Principal set-up for measurements of the NLO properties.

2.3. Non-linear optical measurements

The measurement set-up for detection of the second-order optical SHG and simultaneous ellipsometric monitoring of the surface is illustrated in figure 1. A pulsed Q-switched nitrogen UV laser ($\lambda = 0.337$ μm) with the same parameters as described earlier is used as the photoinducing beam (pump beam). Its power parameters are detected using a photomutiplier **PM4** connected to a electronic boxcar integrator with a gate varying within 400–1000 ps. Polarizer **P1** together with dielectric mirrors **M1** define the laser beam polarization directions of the photoinducing beam. The angle of incidence of the pump beam is varied within 2.6°–8.4° depending on the efficiency of the output signal. The beam spot of the laser usually has a diameter which varies within the range of 80–600 μm. The system of mirrors **M1** allows continuous variation of the diameter of the beam spot and operation by power densities of the photoinducing beam within 0.1–2.1 GW cm^{-2} per pulse. A Gd^{3+}:YAB pulse laser (with wavelength $\lambda = 1.76$ μm) temporally synchronized with the photoinducing nitrogen laser beam is used to produce the probing (fundamental) laser beam. This gives the possibility of generating short laser pulses within a period of 7–30 ps when the pump peak power equals ∼2–8 MW and the pulse repetition frequency is about 11 Hz. The output SHG signal was verified by the parabolic dependence of the fundamental pump beam.

The beam diameter was around 20–50 μm, and was completely overlapped (shot) by the photoinducing laser. The time duration of the pulses was chosen in such a way as to avoid overheating of the samples. The propagation of the fundamental laser beam was perpendicular to the sample surfaces. The delaying line (**DL**) served for the retardation of probing beams with respect to the pumping one. The intensity of the fundamental laser beam was monitored using the photomultiplier **PM3** and a polarizer P1 to define its polarization state. Polarizer **P3** was used to investigate different light polarizations propagating through the specimens (**Sp**). A grating spectrophotometer (**SP**) (with a spectral resolution of about 0.7 nm mm^{-1}) was used to study the intensity of the output doubled-frequency SHG signal (possessing wavelength $\lambda = 0.88$ μm). The delaying line and the pumping and probing laser pulses were connected through the electronic boxcar integrator with photomultipliers **PM1** and **PM2** monitoring the output SHG signal as well as scattered background. The sample was rotated to obtain the angle-dependent SHG behaviour necessary for estimation of the effective second-order optical susceptibilities. The latter were treated like the Maker fringe maxima. At the same time, near-surface photoinduced processes were monitored independently by photoinduced ellipsometry (for convenience the first channel of the ellipsometer is indicated by **E1** and the second one registrated **EPM** is connected with the photomultiplier).

During the evaluation of the pump–probe SHG response, we performed measurements of light intensities at 2ω laser frequencies with a time increment of 0.6 ps. This was achieved using the electronic boxcar integrator under time-synchronized pump–probe conditions. Calculations of the second-order susceptibilities χ_{ijk} were conducted using the following expression:

$$I(\omega, t) = \frac{2\mu_0^{3/2}\varepsilon_0^{3/2}\omega^2\chi_{ijk}^2 I(\omega, t-\tau)^2}{\pi R_0^2 n(2\omega)n^2(\omega)}\left[\frac{\sin(\frac{\mathrm{d}\,\Delta k(t)}{2})}{\frac{\mathrm{d}\,\Delta k(t)}{2}}\right]^2, \quad (1)$$

where R_0 is the radius of the fundamental light beam which possesses a Gaussian-like profile; ε_0 and μ_0 are the dielectric

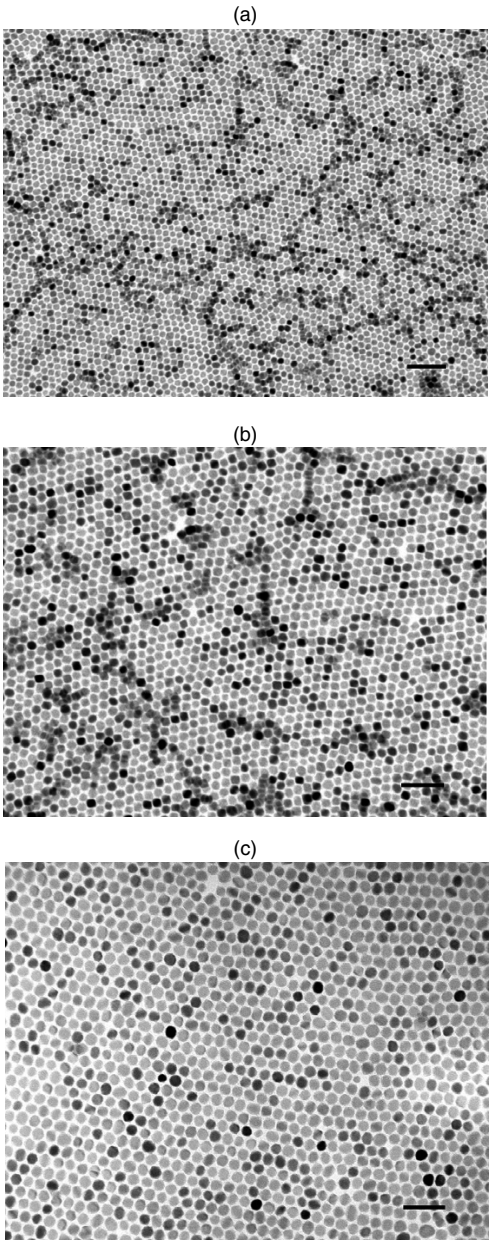

Figure 2. TEM images, recorded from (a) 0193C (top), 0925F and 1004B (bottom), respectively. Each bar represents 100 nm.

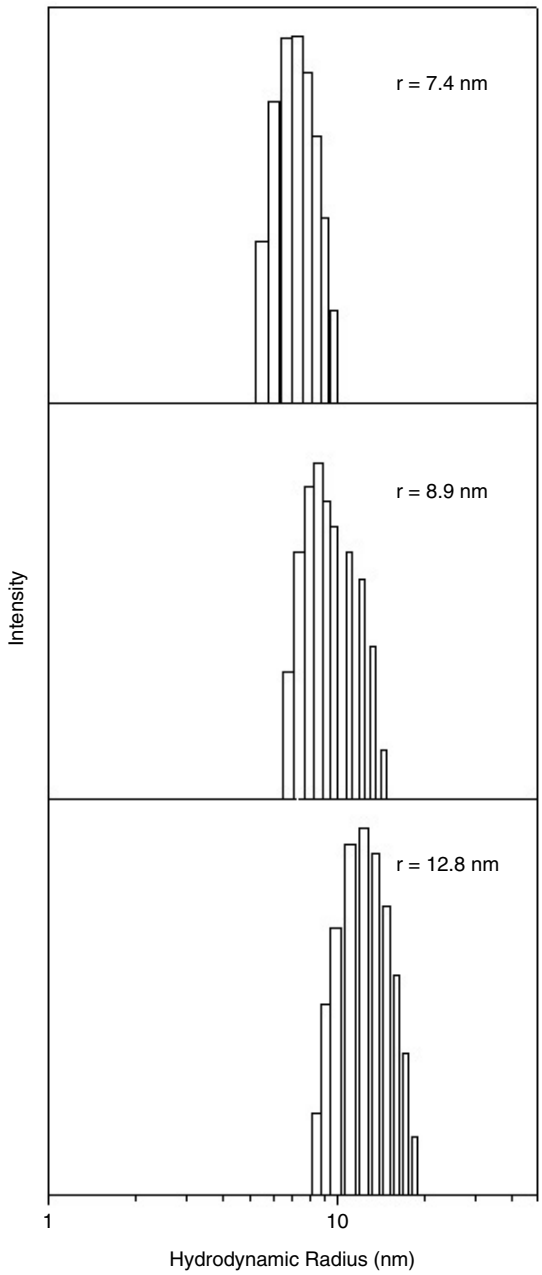

Figure 3. Crystalline size distributions of samples (a, top) 0913C, (b) 0925F and (c, bottom) 1004B.

and magnetic permittivity of a vacuum; τ is the pump–probe delaying time; $n(2\omega)$ and $n(\omega)$ are refractive indices for the fundamental and SHG doubled frequency beams, respectively; χ_{ijk} denotes a component of the second-order NLO susceptibility; $\Delta\mathbf{k}(t) = \mathbf{k}(2\omega) - 2\mathbf{k}(\omega)$ is a phase matching coefficient.

3. Results and discussion

3.1. Size and phase verification

Figures 2(a)–(c) shows transmission electron microscope (TEM) images of samples 0913C, 0925F and 1004B, respectively, demonstrating high quality in morphology and narrow distribution in size (low size dispersion or high monodispersion). From these short-range close-packed patterns, we have determined that the average diameters for three samples were about $\sim 14 \pm 0.8$ nm, $\sim 18 \pm 0.9$ nm and $\sim 24 \pm 1.1$ nm, respectively. The standard deviation of crystalline size for any of the three samples was calculated as no larger than $\sim 6\%$. To verify the size determined from TEM we also conducted light scattering measurements on three samples. Figures 3(a)–(c) present the radius distribution of three In_2O_3 nanocrystal samples. On the basis of light scattering measurements, the mean radii of 0913C, 0925F and 1004B were calculated to be equal to 7.4, 8.9 and 12.8 nm, respectively. These results are in good agreement with those from our TEM observation. For all of the In_2O_3 samples,

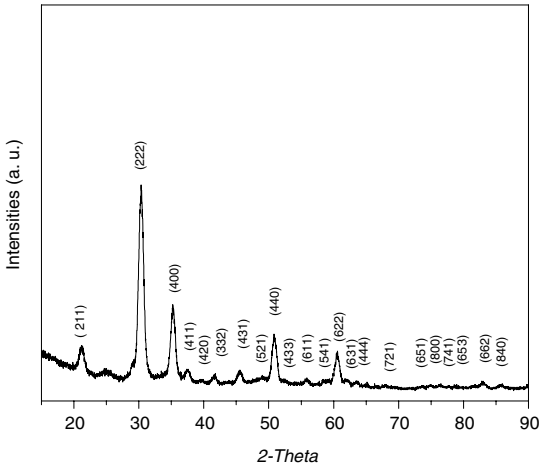

Figure 4. X-ray powder diffraction pattern of In_2O_3 sample 0913C.

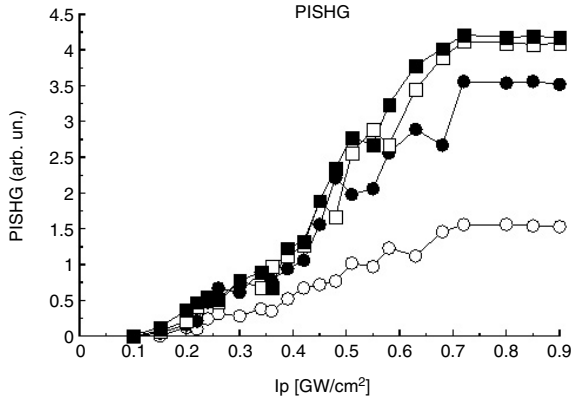

Figure 5. Pump dependence of the second-order susceptibility for In_2O_3 nanocrystals of different sizes: open rings, sample 0913C (14 nm); closed rings, 0925F (18 nm); closed squares, 1004B (24 nm); open squares, 1105F (11–12 nm).

x-ray diffraction (XRD) investigation indicates a cubic phase because all of the detectable diffraction peaks in each pattern are indexed to those from body-centred cubic In_2O_3 (ICDD PDF card Nno 06-0416). As an example, the XRD pattern recorded on sample 0913C is shown in figure 4, in which the average size of crystallites estimated by applying the Scherrer equation [23] is close to that calculated from the TEM image (figure 2(c)).

There is no difference between this XRD trace and that recorded from bulk In_2O_3 concerning the positions of all the detectable peaks. However, the peaks presented in this pattern seem widened, indicating the formation of nanoscale particles.

3.2. Non-linear optical investigation and the role of nanointerfaces

Figure 5 presents the experimental dependences of the photoinduced SHG versus pump power density of the pumping nitrogen laser. Efficient second-order optical susceptibility increases with a decrease of the sizes of LSNC from 24 to 11 nm, suggesting that further decrease of the sizes should drastically suppress the corresponding susceptibility. However, careful investigations on samples with sizes of ∼11–12 nm (see figure 5) show a small decrease in the corresponding susceptibilities. Generally the value of optical nonlinearity is almost one order higher than for the nanolayers separating the films and substrate [16, 18]. Figure 5 clearly exhibits a saturation of the photoinduced SHG measured on all investigated samples. It is crucial that the SHG saturation appears almost at the same pumping power density (at about 0.6 GW cm^{-2}) and for the monodisperse samples the SHG signal substantially increases as the size of the sample decreases. It is important that an enhancement of the sample size dispersion, even by a few per cent, leads to a substantial decrease of the output SHG signal. Another important fact is the suppression of the NLO effect in the powders made using the traditional Kurtz–Perry powder method. This fact may additionally confirm the crucial role played by nanointerfaces, since the corresponding susceptibility was enhanced [19] when the pure nanoconfined effect was investigated. Figure 5 clearly shows the existence of d_{eff} saturation, which appears when the volume of the reconstructed surface is commensurate with the bulk-like volume of the crystallites. It is well known that in the centrosymmetric bulk crystals the second-order effect described by third-order polar tensors is forbidden by symmetry. Therefore, one of the sources of the non-centrosymmetry may be the reconstructed level of the interface. In order to prove this prediction, we carried out calculations of the space distribution of the charge density. Using the TEM inputs, we performed simulations of the space distribution of the local charge density for the local In–O structural clusters.

In [15], it was shown that a crucial role in the observed optical susceptibilities of the LSNC is played by the reconstructed interface sheets of the LSNC, which are1–3 nm thick based on information from TEM and NMR studies. One can therefore expect the appearance of a reconstructed near-surface structure possessing structural near-surface crystalline conformations corresponding to thermodynamically metastable (or even unstable) states. In order to achieve a structural conformation corresponding to the minimum of the total energy, the structure should be optimized using different molecular dynamics methods and various principal structural parameters (bond lengths, angles, torsion angles etc). For LSNC, the principles of long-range ordered translation symmetry of bulk-like perfect crystallites as a consequence of the Bloch rule could also be applied. The perturbation of such an initial layer will be manifested through changes in atomic positions. Since we have at least five to seven layers of perfect long-range ordered crystal (which are fixed) and only the addition (mixture) of one disordered (perturbed) layer, which is under modification, the first reconstructed layer structure (the optimized one) presents a slightly modified crystal structure. Afterwards this modified layer is augmented to the perfect crystal structure and the procedure is repeated for the next layer iteratively. The process looks to be iterative with respect to total energy as a varied parameter. The main criterion is achievement of the minimum of the total energy during such an iteration procedure. Afterwards this procedure is repeated iteratively until the total energy difference between the two next step-by-step-modified layers is less than 0.15 eV. In order to avoid jumps of the potential at the borders, an additional derivative procedure was

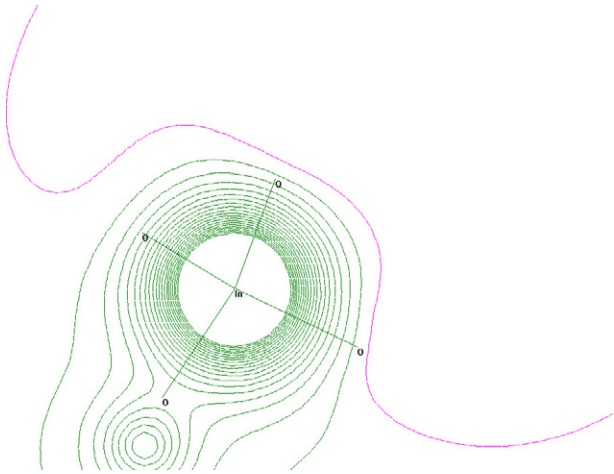

Figure 6. Local charge density distribution of the In_2O_3 NC on interfaces at a photoinducing nitrogen pump power density of about 0.65 GW cm^{-2} for samples with sizes of 24 nm. The isoelectron surface lines correspond to 0.05 e Ω^{-1}.

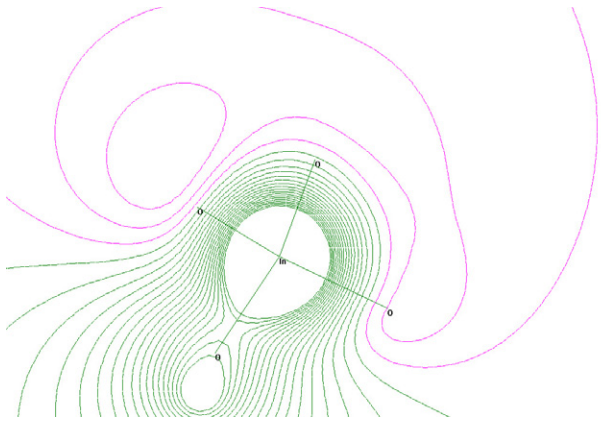

Figure 7. The same as figure 6 for a sample of size 14 nm.

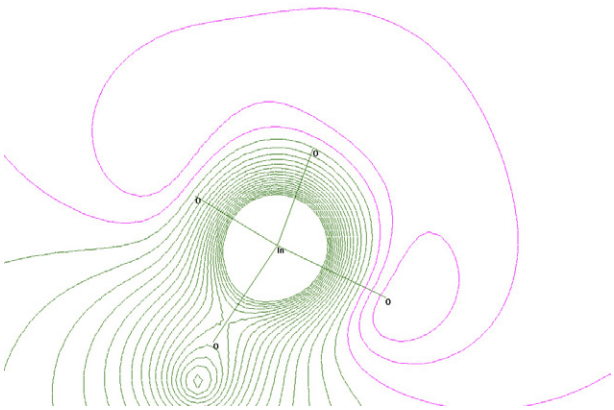

Figure 8. The same as figure 6 for a sample of size11 nm.

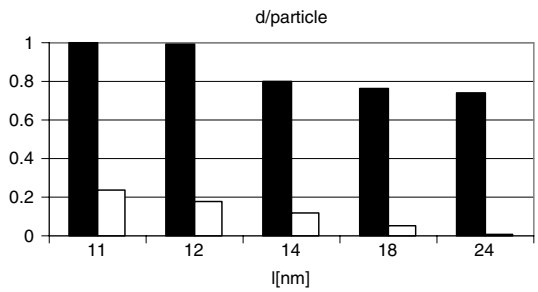

Figure 9. Dependence of the optical nonlinearity per nanoparticle for two different matrices: black, PMMA matrix; white, oligoetheracrylate photopolymer matrix. The maximum optical nonlinearity achieved for the PMMA incorporated chromophore is taken as a reference for the performed calculations.

developed and performed for the potential. Among the various molecular dynamics approaches applied, the most appropriate one is Becke's method. This approach gives the possibility of including dipolar interactions between the chromospheres and the surrounding dipole moments for the polymer host. Finally, it is believed that a structural cluster consisting of 50–70 atoms corresponding to clusters with six to eight layers of reconstructed surfaces reflects relatively stronger changes of electrostatic potential on the boundaries separating the crystallites and surrounding background compared with the monophase regions. Usually static as well as transition dipole moments within the reconstructed layer seem to prevail in the observed dependences. Introducing an appropriate weighting factor into the appropriate structural form-factor (for determination of the particular crystalline structures) of the secular equation, we perform evaluations of the band energy dispersion for perfect crystalline states perturbed by interfaces. As a consequence, a substantially flatter energy dispersion in the k-space is observed.

Figures 6–8 indicate space redistribution of the charge density in the principal LSNC structural cluster at a pumping power density of ~0.6 GW cm^{-2}, showing that decreasing the nanocrystalline sizes and related radius favours an enhanced non-centrosymmetric local density, directly relating to the second-order susceptibilities. Therefore, these interface nanolayers and nanoquantization within the NCs have important roles.

Comparing figure 7 with figure 8 one can see that the effect is not enhanced with decreasing size of the NC. However, the degree of non-centrosymmetry of the space charge density is substantially changed. These results demonstrate the major role of nanointerfaces on the borders separating the LSNC and the surrounding polymer background. To verify the role of the surfaces, we also conducted additional measurements when the NCs were incorporated into highly polarized photopolymer oligoetheracrylate matrices [24]. These matrices may substantially renormalize values of the interface dipole moments, and provide information about second-order susceptibilities.

Figure 9 presents the size dependences of the corresponding second-order susceptibilities for the nanocrystallites incorporated into the PMMA and photopolymer matrices, revealing a substantial suppression of the second-order optical effects in the highly polarized photopolymer matrices compared with the slightly polarized (almost polarization neutral) PMMA matrices. This may be a consequence of the compensation by the photopolymer matrices of the near-surface dipole moments originating from the charge density distribution at the interface.

It is necessary to emphasize again that there is a difference between metallic nanoparticle systems [19] and the current In_2O_3 system. In the former, an important role is played by surface-plasmon resonance and the susceptibility should vary as the inverse third power of the radius, whereas in the latter quantum-confined effects near the interfaces pay a significant role.

4. Conclusions

A drastic increase in the second-order optical susceptibilities was observed in large-size monodisperse In_2O_3 NCs with incorporated into PMMA polymer matrices. As the size of LSNCs decreased from 24 to 11 nm, efficient second-order optical susceptibility increased, suggesting that a further decrease in size should drastically suppress the corresponding susceptibility. However, careful investigations on samples of size ∼11–12 nm reveal a small decrease in the corresponding susceptibilities. Replacement of slightly polarized PMMA matrices by highly polarized oligoetheracrylate photopolymer matrices demonstrated a drastic suppression of the NLO effect. The same suppression was observed when size dispersion was narrowed. This confirms the substantial role of the near-interface states in the observed NLO features.

Generally the value of the optical nonlinearity for NC incorporated into the PMMA matrices is almost one order higher than for the nanolayers separating the films and substrate. This fact may reflect a crucial role for nanointerfaces in the observed effect, because the corresponding susceptibility should be enhanced based on the quantum-confinement effect of the pure NCs. The theoretical calculations performed within the framework of the band energy structure approach together with the interface molecular dynamics simulations indicate a major role of the interfaces in the effect observed.

The effect observed here is different in principle from that observed in the metallic nanoparticle system [19]. In each case the quantum-confined enhancement and the surface plasmon resonances are substantially different.

Acknowledgments

This work was supported by NSF CAREER Program (DMR-0449580), NSF NER program (DMI-0508412) and DARPA HR0011-05-1-0031.

References

[1] Wang Q D, Xu J F and Xie R H 2004 Nonlinear optics of nanoparticles and nanocomposites *Encyclopedia of Nanoscience and Nanotechnology* vol 8, ed H S Nalwa (NY, USA: American Scientific Publishers) pp 100–10
Cui Y and Lieber C M 2001 *Science* **291** 81–93
[2] Li A P, Flack F, Lagally M C, Chishom M F, Yoo K, Zhang Z, Weitering H H and Wendelken J F 2004 *Phys. Rev.* B **69** 245310
[3] Brunner K 2002 *Rep. Prog. Phys.* **65** 27–72
[4] Schmidt O G, Lange C and Eberl K 1999 *Appl. Phys. Lett.* **75** 1905–7
[5] Takayuki H and Takuya O 2004 *J. Colloid Interface Sci.* **273** 471–7
[6] Buckner S W, Konold R L and Jelliss P A 2004 *Chem. Phys. Lett.* **394** 400–4
[7] Alivisatos A P 1996 *Science* **271** 933–7
[8] Ellert C, Schmidtr M, Reiners T and Haberland H 1997 *Z. Phys.* D **39** 317–27
[9] Hill N A and Whaley K B 1996 *Chem. Phys.* **210** 117–33
[10] Kityk I V 2003 *Semicond. Sci. Technol.* **18** 1001–9
[11] Shuan K 2004 *Reports on Chem. Biophysics*; *Chin. Chem. Bulletin* 314
[12] Su H, Xie Y, Gao P, Xiong Y and Qian Y 2001 *J. Mater. Chem.* **11** 684–6
[13] Boucle J, Kassiba A, Emery J, Kityk I V, Makowska-Janusik M, Sanetra J, Herlin-Boime N and Mayne M 2002 *Phys. Lett.* A **302** 196–202
[14] Mavi H S, Sudakshina P, Shukla A K and Abbi S C 2003 *Opt. Commun.* **226** 405–13
[15] Kityk I V 2001 *J. Non-Cryst. Solids* **297** 234
[16] Ebothé J, Kityk I V, El Hichou A, El Idrissi B, Addou M and Krasowski J 2003 *J. Vac. Sci. Technol.* A **21** 201–5
[17] Kityk I V, Majchrowski A and Sahraoui B 2005 *Opt. Lasers Eng.* **43** 75–83
[18] Kityk I V, Ebothe J, Miedzinski R, Addou M, Sieber H and Karafiat A 2003 *Semicond. Sci. Technol.* **18** 549–53
[19] Hache F, Ricard D and Flytzanis C 1986 *J. Opt. Soc. Am.* B **3** 1647–55
[20] Kityk I V, Makowska-Janusik M, Gondek E, Krzeminska L, Danel A, Plucinski K J, Benet S and Sahraoui B 2004 *J. Phys.: Condens. Matter* **16** 231–9
[21] Liu Q, Lu W, Ma A, Tang J, Lin J and Fang J 2005 *J. Am. Chem. Soc.* **127** 5276–7
[22] Migalska-Zalas A, Makowska-Janusik M, Kityk I V, Sahraoui B, Salle M and Gorgues A 2003 *Acta Phys. Pol.* **103** 293–300
[23] Cullity B D 2005 *Elements of X-ray Diffraction* 2nd edn (Reading, MA: Addison-Wesley)
[24] Majchrowski A, Mefleh A, Lee R, Makowska-Janusik M, Kasperczyk J, Kityk I V, Berdowski J and Benet S 2000 *Nonlinear Opt.* **24** 335–50